Article

Micromechanical analysis of longitudinal and shear strength of composite laminae

Lucas L Vignoli[1,2], Marcelo A Savi[1], Pedro MCL Pacheco[3] (iD) **and Alexander L Kalamkarov[4]** (iD)

Abstract
The analysis of several micromechanical models for estimating strength of composite laminae is presented. Longitudinal tensile, compressive and in-plane onset shear strengths are analytically estimated and compared with experimental data available in the literature. The tensile longitudinal load predominantly induces rupture of fibers. On the other hand, the compressive strength is highly influenced by fiber misalignment, inducing a wide range of failure mechanisms. The material response to in-plane shear presents a strong nonlinear response. The estimation of longitudinal tensile strength based on the rule of mixture approaches is compared with 27 experimental data. A novel improvement is proposed assuming that *in situ* strength of fiber is smaller than fiber strength measured individually due to manufacturing induced damage. For the in-plane shear, 6 models are compared with 10 experimental stress-strain curves, including a novel closed-form expression based on the concentric cylinders model. Finally, for the longitudinal compressive strength, 8 micromechanical models, including a novel model to estimate misalignment effect in fiber crushing, are compared with 61 experimental data are analyzed. Results indicate that the minimal average error for the longitudinal tensile strength is 12.4% while for the compressive strength it is 15%. For the shear strength, the closest prediction depends on the strength definition and the proposed damage onset strength presents the best predictions. In general, the newly proposed models present the best estimations compared with the other models.

Keywords
Composite material, unidirectional laminae, micromechanics, analytical modelling, longitudinal tensile, compressive and in-plane strengths

Introduction

Strength of composite laminates has been widely investigated in the last decades and a considerable advance in failure modeling is obtained, especially due to the World Wide Failure Exercise (WWFE).[1–3] The WWFE is an international effort to compare different failure criteria where fibers, matrices, laminae, lay-up and load are provided by the organizers and the participants have to estimate the failure characteristics. Among the participants, just the Chamis model[4] uses an analytical micromechanical approach to compute the properties of the homogenized laminae. The Bridging model is also compared with the same set of experimental data independently.[5] Some other participants use numerical homogenization procedures or just the effective properties of the laminae, without any homogenization step. Nevertheless, lamina equivalent properties are valid only for the specific fiber volume fraction and provides limited information for design optimization. For practical applications, new test for each value of fiber volume fraction is prohibitive.[6] On the other hand, the computational cost for numerical modeling is also a big issue.[7] Hence, the analytical

[1]Department of Mechanical Engineering, Center for Nonlinear Mechanics, COPPE, Universidade Federal do Rio de Janeiro, Brazil
[2]Department of Mechanical Engineering, Center for Technology and Application of Composite Materials, Universidade Federal do Rio de Janeiro, Brazil
[3]Department of Mechanical Engineering, Centro Federal de Educação Tecnológica Celso Suckow da Fonseca CEFET/RJ, Brazil
[4]Department of Mechanical Engineering, Dalhousie University, Canada

Corresponding author:
Alexander L Kalamkarov, Dalhousie University, PO Box 15000, Halifax, NS B3H 4R2, Canada.
Email: alex.kalamkarov@dal.ca

formulations become a fundamental tool for parametric and optimization analyses.

Regarding the micromechanical modeling, two main steps are required: the computation of effective elastic properties and macromechanical strength. For the effective elastic properties, a detailed discussion is presented by Vignoli et al.[8] Strength analysis is associated with different failure mechanisms and needs to be established by several experimental tests. As a starting point, it is important to define longitudinal and transversal strengths. Concerning experimental tests, six macroscopic strengths are required based on the coordinate system shown in Figure 1, where the direction x_1 coincides with the fiber orientation and the plane $x_2 - x_3$ is transversal to the fiber: longitudinal tension, S_{11}^t; longitudinal compression, S_{11}^c; transversal tension, S_{22}^t; transversal compression, S_{22}^c; longitudinal shear, S_{12}^s; and transversal shear, S_{23}^s.

This paper considers micromechanical models for the estimation of macroscopic longitudinal tensile S_{11}^t, compressive S_{11}^c and in-plane shear S_{12}^s strengths. The property S_{12}^s is specified as in-plane shear strength, but it could be denoted as axial shear strength as well. Additionally, the fibers' distribution is assumed symmetric in plane $x_2 - x_3$, and therefore, the lamina is transversally isotropic, which means that $S_{12}^s = S_{13}^s$, $S_{22}^t = S_{33}^t$ and $S_{22}^c = S_{33}^c$. The macroscopic transversal strength of composite laminae is analyzed in Vignoli et al.[9]

An important point to be highlighted concerning longitudinal strength is based on the unit circle modeling approach proposed by Tsai and Melo.[10] For a given laminate subjected to uniaxial load, the final failure is assumed to be dependent on the plies where the fibers are oriented parallel to the load direction. For any plane stress load condition, the failure can be determined by a unit circle on the normalized strain plane. As the most popular laminates are designed based on the ten-percent rule,[11] plies oriented with 0° and 90° are assumed to define the failure. In other words, just the longitudinal tensile and compressive strengths are required to design composites with this approach. However, some compressive strength models require shear strength as input.
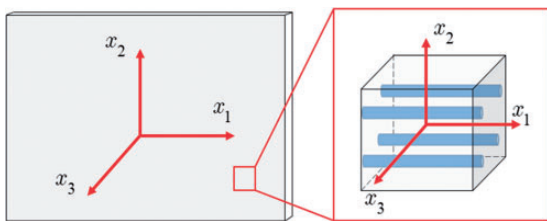

Figure 1. Definition of coordinate systems used to define the materials properties.

Hence, these three strengths can be considered as the key points to model composite failure based on Tsai and Melo theory.

This paper presents a general overview of the micromechanical models for longitudinal strength and it proposes novel alternatives. The estimation of macroscopic strength is based on the properties of the constituents: fibers and matrix. Based on the WWFE constituents input properties, the following set of properties are assumed to be known: fiber longitudinal and transversal elastic moduli, E_1^f and E_2^f; fiber longitudinal and transversal shear moduli, G_{12}^f and G_{23}^f; fiber longitudinal Poisson's ratio, ν_{12}^f; fiber tensile and compressive strengths, S_t^f and S_c^f; matrix elastic modulus, E^m; matrix Poisson's ratio, ν^m; matrix tensile, compressive and shear strengths, S_t^m, S_c^m and S_s^m. Regarding tensile strength, the classical estimation based on the ROM is discussed and a new parameter is introduced to evaluate the fiber *in situ* strength reduction. Although the fiber strength reduction is discussed in the literature,[12] an average analysis useful for practical design applications is proposed. The onset shear strength analysis considers a closed-form expression based on the concentric cylinders model. Despite the concentric cylinders model is not novel,[13] the expression derived in the present paper is a new contribution. Regarding the compressive strength, the fiber misalignment is included in the criterion, assuming a polynomial form model that allows the use of simple equations.[14] Due to curvature effect, the misalignment decreases lamina compressive strength and the proposed model is able to quantify it.

After this Introduction, further discussion on each of the strengths is presented, highlighting the associated literature. The next section discusses the longitudinal tensile strength comparing results with 27 experimental data. The novel model proposed in this paper presents the simplest modeling with a good prediction capability compared with the other approaches. Then, a discussion about in-plane shear strength is presented, including some issues regarding shear strength definition. Six models are discussed and compared with 10 experimental stress-strain curves. The novel longitudinal onset shear is proposed on a closed-form expression derived based on the concentric cylinders modeling technique. The longitudinal compressive strength is investigated in the penultimate section. This specific strength is related to a considerable disagreement among models due to different failure mechanisms. Eight analytical models are discussed for this strength and 61 experimental data are compiled for the analysis. The novel model includes the misalignment effect of the fiber crushing failure and presents good results. The main conclusions and recommendations are presented in the final section.

Longitudinal tensile strength

A composite made of fibers and matrix, subjected to tensile longitudinal stress, σ_{11}, has the essential characteristic that fibers and matrix works like elements in parallel. In a general sense, the estimation of the macromechanical strength considers that the load sharing must be computed in order to evaluate if the stress on the fiber, σ_{11}^f, or the stress on the matrix, σ_{11}^m, can result in failure.

Assuming that the failure takes place when the stress on the fiber is equal to its tensile strength, the macromechanical and micromechanical points of view are equivalent to $\sigma_{11} = S_{11}^t$ and $\sigma_{11}^f = S_t^f$, respectively. Based on the ROM, both constituents have the same strain due to geometrical compatibility and considering the linear elastic behavior until failure, the longitudinal tensile strength is estimated by

$$S_{11}^t = \left[V_f + (1 - V_f)\left(\frac{E^m}{E_1^f}\right) \right] S_t^f \quad (1)$$

where V_f is the fiber volume fraction, E^m is the matrix elastic modulus, E_1^f is the fiber longitudinal elastic modulus.

Novel approach

The manufacturing damage seems to be a relevant aspect to define the longitudinal tensile strength. According to Barbero,[12] experimental results indicate fiber *in situ* strength decreasing up to 53% for glass fibers and up to 30% for carbon fibers. In order to evaluate this effect, a fiber strength reduction parameter, r, is proposed to obtain a value that minimizes the average error of the estimations using equation (1) and the experimental data compiled from references. The following equation is proposed

$$S_{11}^t = \left[V_f + (1 - V_f)\left(\frac{E^m}{E_1^f}\right) \right] (1 - r) S_t^f \quad (2)$$

Alternatively, the fiber strength reduction parameter, r, can be computed from a longitudinal tensile strength experimental data using the following equation:

$$r = 1 - \frac{S_{11}^t}{S_t^f}\left[V_f + (1 - V_f)\left(\frac{E^m}{E_1^f}\right) \right]^{-1} \quad (3)$$

Comparative analysis

A set of 27 experimental data compiled from 13 references (see Table 1 and Table 4 in Appendix 1) is used in

Table 1. References used for the experimental data of the longitudinal tensile strength, S_{11}^t.

| Reference	Fiber type
Aboudi[15]	Carbon
Barbero et al.[16]	Carbon
Bogdanor et al.[17]	Carbon
Falcó et al.[18]	Carbon
Hsiao and Daniel[19]	Carbon
Jumahat et al.[20]	Carbon
Kaddour and Hinton[21]	Carbon and glass
Kaddour et al.[22]	Carbon and glass
Namdar and Darendeliler[23]	Carbon
Perogamvros and Lampeas[24]	Carbon
Reddy et al.[25]	Carbon and glass
Soden et al.[26]	Carbon and glass
Wang et al.[27]	Carbon
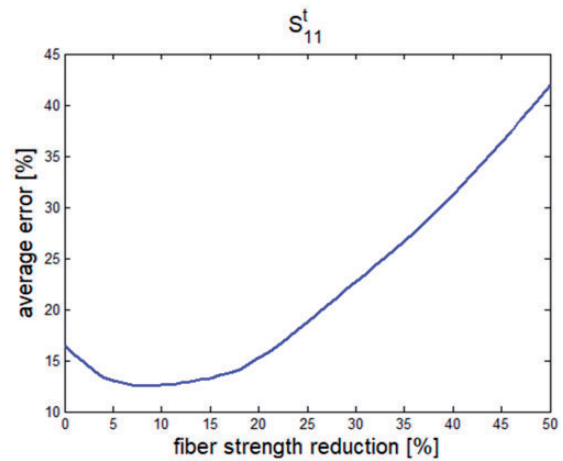
Figure 2. Average error for the longitudinal tensile strength, S_{11}^t.

order to evaluate the tensile strength. The idea is to compare model predictions considering two different approaches: the absolute value of the average error; and the ranges of error, which are classified as smaller than 10%, between 10% and 20%, between 20% and 30%, between 30% and 40%, between 40% and 50% and higher than 50%.

The average error according to r is presented in Figure 2 showing an average error of 16.5% for $r = 0.00$ and 12.5% for $r = 0.08$, indicating a small improvement using the parameter r. Figure 3 shows a comparison of the error range for $r = 0.00$ and $r = 0.08$. Note that 59.3% of the cases have an estimation with error smaller than 10% for $r = 0.00$. On the other hand, 63% of the cases have an estimation with error smaller than 10% for $r = 0.08$.

Figure 4 shows a comparison of the different values of r computed from the equation (3) with all the
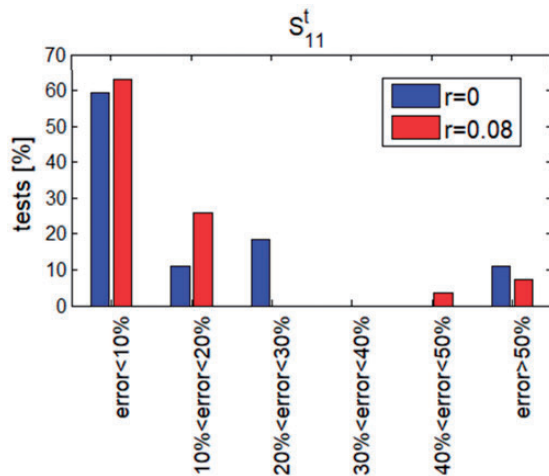
Figure 3. Ranges of error for the longitudinal tensile strength, S_{11}^t.
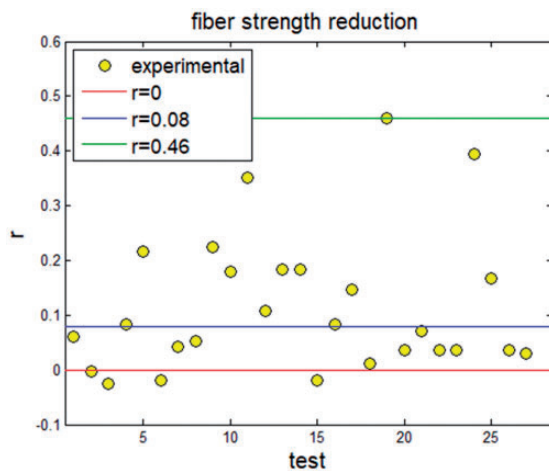

Figure 4. Fiber strength reduction for all the compiled experimental data.

experimental data compiled. This result indicates the large variation of r according to the experimental data, highlighting the classical ROM estimation ($r = 0$), the average value ($r = 0.08$) and the upper bound from compiled experimental data ($r = 0.46$). Additionally, it is worth noting that among 31 experimental data there are 4 indication of negative values of r ($r = -0.002$, $r = -0.024$, $r = -0.019$ and $r = -0.02$). This result cannot be interpreted assuming that fiber strength increases *in situ*, but it is due to high dispersion of the fiber strength and its statistical nature. Note that fiber strength is an average value from a set of experimental data obtained testing a large number of fibers individually.

As fibers embedded in a matrix work like a bundle, it is impossible to say that all fibers fail (break) under the same load. Based on this observation, some authors have been modeling the fiber damage using a Weibull distribution.[28,29] Some issues related to the use of Weibull distribution to describe the fiber damage are discussed in literature.[30,31] It should be noted that size influences the fiber strength,[31] as expected by classical strength of materials.[32] This study is concerned with macromechanical strength models and further investigation of these topics is out of the scope of the present paper.

In-plane shear strength

Lamina subjected to shear load in plane x_1–x_2 presents a strong nonlinear behavior due to matrix damage propagation.[33] The first issue on the description of this nonlinearity is the difficulty to apply pure and uniform shear load. ASTM D4762-18[34] summarizes 5 tests proposed to measure longitudinal shear modulus and strength. Each test has an individual standard, but the shear strengths definition is the same for all of them.

Different kinds of strengths can be defined to evaluate the model assumptions. *Offset shear strength*, $S_{12}^{s,0.2\%}$, defined by the point where a line parallel to the shear modulus with offset in 0.2% on the shear strain axis, crosses the the experimental stress-strain curve. This definition is similar to the yield strength for metals. *Shear strength* or *rupture shear strength*, $S_{12}^{s,r}$, defined as the minimum value between the rupture stress and the stress when the shear strain is equal to 5%. These two definitions are associated with ASTM standard. Another strength definition proposed in this paper is the *onset shear strength*, $S_{12}^{s,o}$, which is the first damage event that can be defined as the start of the nonlinear behavior of the stress-strain curve.

The material nonlinear response can be understood by two different ways. From plasticity theory, the matrix damage propagation is associated with the increase of the matrix yield area.[35] On the other hand, fracture mechanics defines the longitudinal shear as the mode II crack propagation,[12] which requires a higher amount of energy to propagate.[36]

Some references employed the two strengths defined by the standards, instead the only rupture shear strength as the most common procedure.[37] For instance, Jumahat et al.[38] reported offset strength equal to 52 MPa and rupture strength equal to 101 MPa for carbon fiber composite, while Laustsen et al.[39] reported 27 MPa and 70 MPa for a glass fiber composite.

The simplest model to estimate the shear strength is based on the rule of mixture (ROM). From micromechanics, matrix damage is defined by $\sigma_{12}^m = S_s^m$, where S_s^m is the matrix shear strength, and lamina damage is represented by $\sigma_{12} = S_{12}^s$. Considering fiber and matrix

as element working in parallel, $\sigma_{12} = \sigma_{12}^m = \sigma_{12}^f$. Hence, the ROM estimation is defined by

$$S_{12}^s = S_s^m \tag{4}$$

Daniel and Ishai[40] proposed the use of the rule of mixture, including the stress concentration effect. This model is named as a rule of mixture with stress concentration (ROM-Kt), being defined by the following equation:

$$S_{12}^s = \frac{S_s^m}{K_\tau} \tag{5}$$

where

$$K_\tau = \frac{1 - V_f[1 - (G^m/G_{12}^f)]}{1 - (4V_f/\pi)^{0.5}[1 - (G^m/G_{12}^f)]} \tag{6}$$

and G^m is the matrix shear modulus and G_{12}^f is the fiber longitudinal shear modulus.

Note that ROM model is not able to distinguish onset and rupture strengths, once the same stress is assumed along the whole matrix. On the other hand, ROM-Kt estimates that the onset strength due to the stress concentration is a local problem.[41]

Devireddy and Biswas[42] presented a numerical study comparing effective elastic and thermal properties of unidirectional composites assuming fiber with square cross section. Results indicate effective properties close values compared with simulation considering circular cross section. Based on this, the representative volume element (RVE) with square fiber is considered as presented in Figure 5.

The RVE is represented by two squares, the fiber with size a and the matrix with external size b, with a fiber volume fraction of $V_f = (a/b)^2$. This RVE can be divided into five parts: the sub-cells 2i, 2ii and 2iii work in series in plane $x_1 - x_2$ to build a cell 2, that is in parallel with the cells 1 and 3; 1, 2i, 2iii and 3 are the matrix and 2ii is the fiber. The equilibrium requirement
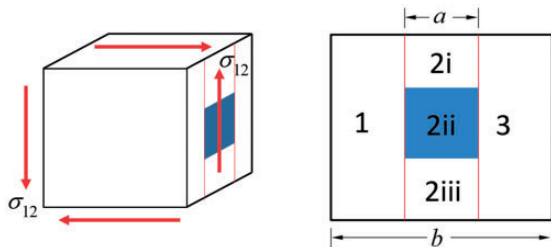

Figure 5. RVE with square fiber submitted to longitudinal shear load.

on the face perpendicular to x_1 is defined by

$$\sigma_{12}b^2 = \sigma_{12}^{(1)}\left[\left(\frac{b-a}{2}\right)b\right] + \sigma_{12}^{(2i)}\left[\left(\frac{b-a}{2}\right)a\right] + \sigma_{12}^{(2ii)}a^2 + \sigma_{12}^{(2iii)}\left[\left(\frac{b-a}{2}\right)a\right] + \sigma_{12}^{(3)}\left[\left(\frac{b-a}{2}\right)b\right] \tag{7}$$

By geometrical compatibility,

$$\varepsilon_{12} = \varepsilon_{12}^{(1)} = \varepsilon_{12}^{(2)} = \varepsilon_{12}^{(3)} \tag{8}$$

where

$$\varepsilon_{12}^{(2)}ab = \varepsilon_{12}^{(2i)}\left[\left(\frac{b-a}{2}\right)a\right] + \varepsilon_{12}^{(2ii)}a^2 + \varepsilon_{12}^{(2iii)}\left[\left(\frac{b-a}{2}\right)a\right] \tag{9}$$

Assuming a linear elastic response of the matrix, cells 1 and 3, and the fiber sub-cell 2ii, the failure is defined by the conditions $\sigma_{12}^{(2i)} = \sigma_{12}^{(2ii)} = \sigma_{12}^{(2iii)} = S_s^m$ and $\sigma_{12} = S_{12}^s$. Manipulating equations (7) to (9), the shear strength is defined by

$$S_{12}^s = \left[\left(1 + V_f - \sqrt{V_f}\right) + \frac{G^m}{G_{12}^f}\left(\sqrt{V_f} - V_f\right)\right]S_s^m \tag{10}$$

Chamis model (Ch)[4] is based on the equation (10), including an additional term due to the effect of volume fraction of voids, V_v, resulting on the following expression:

$$S_{12}^s = \left[1 - \sqrt{\frac{4V_v}{\pi(1 - V_f)}}\right] \times \left[\left(1 + V_f - \sqrt{V_f}\right) + \frac{G^m}{G_{12}^f}\left(\sqrt{V_f} - V_f\right)\right]S_s^m \tag{11}$$

Huang[43] proposed the Bridging model (Br) using the following expression:

$$S_{12}^s = \left[V_f\frac{G_{12}^f}{0.45G_{12}^f + 0.55G^m} + (1 - V_f)\right]S_s^m \tag{12}$$

Recently, Huang[44] proposed a modification of the Bridging model including the stress concentration effect (Br-Kt) by

$$S_{12}^s = \frac{S_s^m}{K_{12}\lambda_4} \tag{13}$$

where

$$K_{12} = \left[1 - V_f\left(\frac{G_{12}^f - G^m}{G_{12}^f + G^m}\right)\left(W - \frac{1}{3}\right)\right]\frac{[V_f + a_{66}(1 - V_f)]}{a_{66}}$$

(14)

$$W = \pi\sqrt{V_f}\left(\frac{1}{4V_f} - \frac{4}{128} - \frac{2}{512}V_f - \frac{5}{4096}V_f^2\right)$$

(15)

$$\lambda_4 = \frac{a_{66}}{V_f + a_{66}(1 - V_f)}$$

(16)

$$a_{66} = 0.3 + 0.7(G^m/G_{12}^f)$$

(17)

Novel approach

A novel approach is proposed based on Zhang and Waas[13] idea, proposing a closed-form expression using the concentric cylinders model (CC). Despite the concentric cylinders model popularity in composite micromechanics,[45] the equation to estimate the onset shear strength developed in this study is not presented in any other publication to the best knowledge of the authors.

The main idea of the method is to impose the displacement field that satisfies the boundary conditions using a RVE build by two concentric cylinders, as represented in Figure 6. The inner cylinder is the fiber, with radius a, and the outer one is the matrix, with internal and external radii, a and b, respectively.
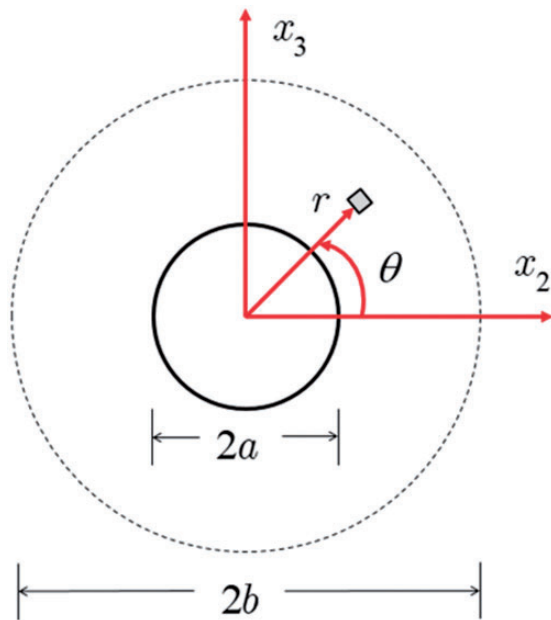

Figure 6. Schematic RVE for concentric cylinders model.

The imposed displacement field in cylindrical coordinates is given by

$$u_x^\kappa = \left(A_\kappa r + \frac{B_\kappa}{r}\right)\cos\theta$$

(18)

$$u_r^\kappa = C_\kappa x\cos\theta$$

(19)

$$u_\theta^\kappa = -C_\kappa x\sin\theta$$

(20)

where $\kappa = f, m$ is used to denote the constituent (fiber or matrix); A_κ, B_κ and C_κ are six constants to be determined, and the longitudinal axis in cylindrical coordinate x coincides with x_1 in Cartesian coordinates.

Using strain definition in cylindrical coordinates[46] and the linear elastic constitutive relation for both constituents, the non-zero stress components are the following

$$\sigma_{xr}^\kappa = G_{12}^\kappa\left(A_\kappa - \frac{B_\kappa}{r^2} + C_\kappa\right)\cos\theta$$

(21)

$$\sigma_{x\theta}^\kappa = -G_{12}^\kappa\left(A_\kappa + \frac{B_\kappa}{r^2} + C_\kappa\right)\sin\theta$$

(22)

In order to avoid singularity, $B_f = 0$. Hence, there are 5 unknown constants. The following compatibility and equilibrium conditions must be satisfied

$$u_x^f(x, a, \theta) = u_x^m(x, a, \theta)$$

(23)

$$u_\theta^f(x, a, \theta) = u_\theta^m(x, a, \theta)$$

(24)

$$u_r^f(x, a, \theta) = u_r^m(x, a, \theta)$$

(25)

$$u_x^m(x, b, \theta) = 0$$

(26)

$$\sigma_{xr}^f(x, a, \theta) = \sigma_{xr}^m(x, a, \theta)$$

(27)

Despite the 5 boundary conditions and 5 unknowns, equations (24) and (25) are linearly dependent. Thus, one additional condition is required. Additionally, equation (26) can only be established based on the dilute composite hypothesis, where the boundary conditions on the outer radius tend to the imposed conditions in a region far from the inclusion. In other words, it is assumed that there is no interaction between neighboring fibers. For a detailed discussion on dilute and non-dilute composites see Andrianov et al.[47] The last equation can be obtained using the strain rotation

$\varepsilon_{12}^{\kappa} = \varepsilon_{xr}^{\kappa}\cos\theta - \varepsilon_{x\theta}^{\kappa}\sin\theta$. Integrating ε_{12} on the RVE

$$\varepsilon_{12}(\pi b^2) = \int_0^a \int_0^{2\pi} (\varepsilon_{xr}^f \cos\theta - \varepsilon_{x\theta}^f \sin\theta) r \mathrm{d}\theta \mathrm{d}r \\ + \int_b^a \int_0^{2\pi} (\varepsilon_{xr}^m \cos\theta - \varepsilon_{x\theta}^m \sin\theta) r \mathrm{d}\theta \mathrm{d}r \tag{28}$$

Based on that, the unknowns are obtained as functions of ε_{12}. Solving the system of equations and defining the failure onset by $\max[\sigma_{12}^m(r,\theta)] = S_s^m$, the shear strain on the failure initiation is given by

$$\varepsilon_{12} = \frac{S_s^m}{4G^m}\left[\frac{G^m(1+V_f) + G_{12}^f(1-V_f)}{G_{12}^f}\right] \tag{29}$$

From the macromechanical point of view, $\sigma_{12} = S_{12}^s = G_{12} 2\varepsilon_{12}$. Using the longitudinal shear modulus derived using the concentric cylinders model,[8] the onset shear strength is

$$S_{12}^s = \frac{S_s^m}{2}\left[\frac{(G_{12}^f + G^m) + (G_{12}^f - G^m)V_f}{G_{12}^f}\right] \tag{30}$$

Comparative analysis

In order to evaluate the model estimations, ten experimental stress-strain curves from the WWFE are employed,[21,22,26] see Tables 5 and 6 in Appendix 1. Figure 7 presents results for glass fiber while Figure 8 shows results for carbon fibers. Based on these results, the main conclusions are:

(i) CC model obtained the closest prediction considering damage onset;
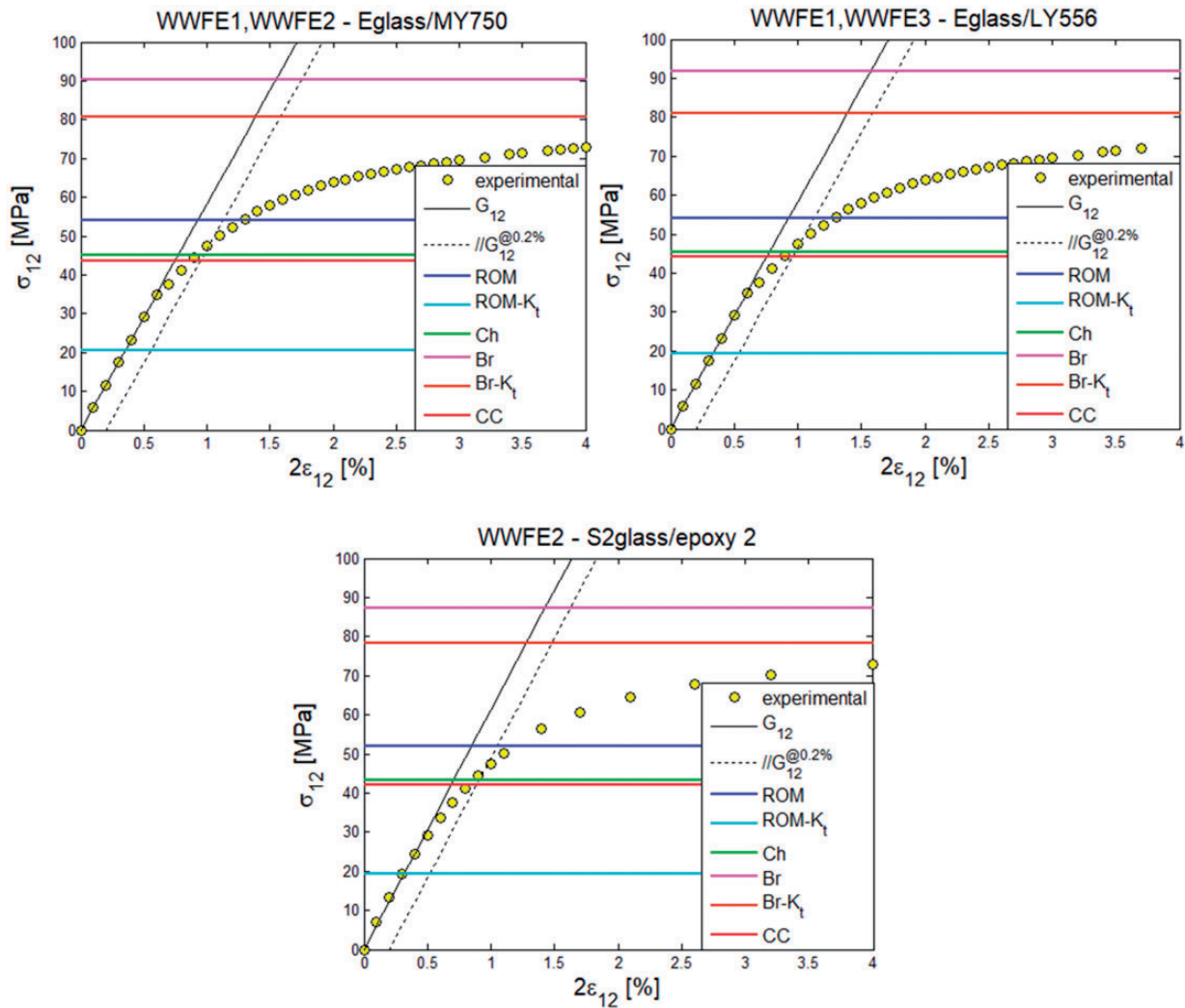

Figure 7. Comparison between the analytical results and experimental data for shear stress-strain curves for glass fibers.[21,22,26]
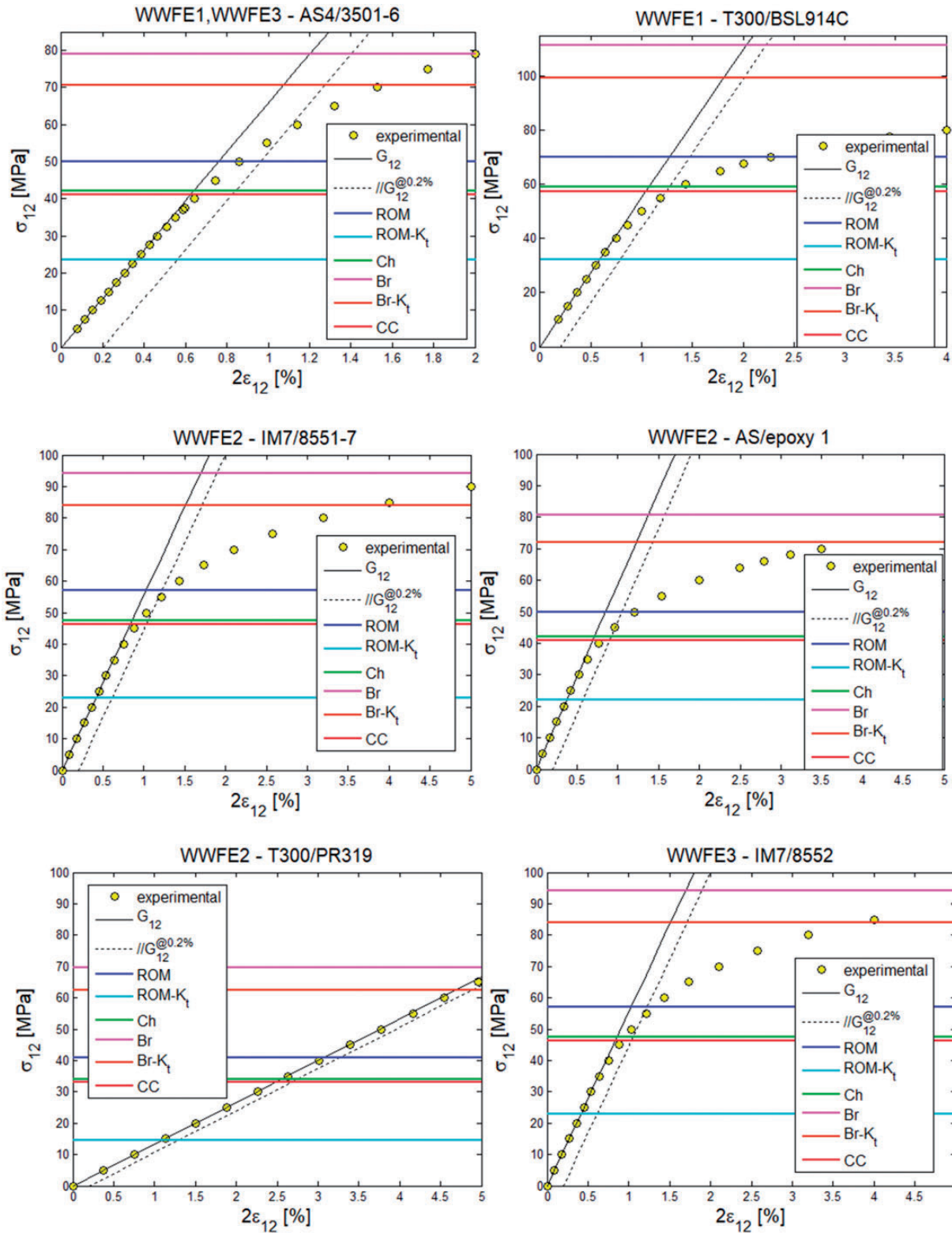
Figure 8. Comparison between the analytical results and experimental data for shear stress-strain curves for carbon fibers.[21,22,26]

(ii) CC and Chamis models tend to have similar estimations;

(iii) Offset shear strength is usually between Ch and ROM models for most of the laminae;

(iv) Br model has the closest estimation for rupture shear strength.

In order to improve the quantitative analysis of shear strength results, Figure 9 shows the average error according to the three shear strength definitions. Note that Br and Br-Kt were developed to estimate ruptures strength, hence they have a poor prediction on the onset and offset strengths. On the other hand, the other models, including the newly proposed CC model, are able to estimate onset strength. This is an important characteristic of the models discussed, once there are different shear strength definitions, each model may be developed to estimate one strength. The proposed CC is the best one to estimate onset shear strength with average error of 31.18%, while Br has the closest estimations for rupture shear strength with average error of 9.11%. The following points should be highlighted:

(i) for the onset strength, $S_{12}^{s,o}$, CC model has the smallest average error (31.18%), but Ch and ROM-Kt also have average error smaller than 40% (34.39% and 39.39%, respectively);

(ii) for the offset strength, $S_{12}^{s,0.2\%}$, Ch has an average error of 14.01% and CC has 15.89%;

(iii) just Br and Br-Kt are proposed to estimate the rupture strength, where the average error comparing with $S_{12}^{s,r}$ are closer to 10%.
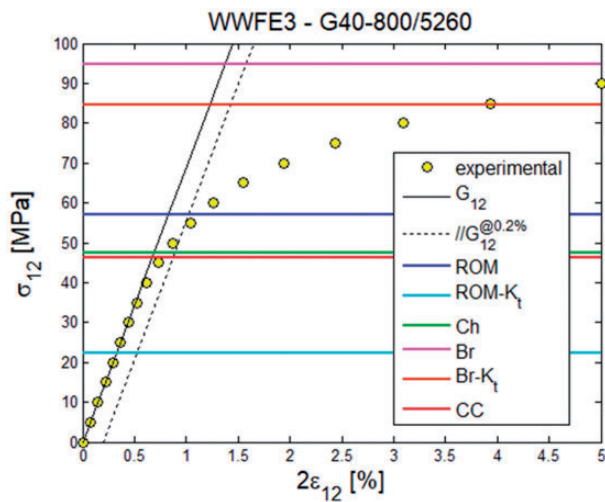
As pointed out by Ha et al.,[33] the micromechanical model must be able to estimate the onset shear strength (or the offset shear strength according to the ASTM notation) and the stress-strain nonlinearity must be considered as damage propagation by appropriated failure criterion. For damage propagation, interface failure may also have an important role. Lamina rupture due to shear load results from two concurrent failure mechanism: damage propagation in the matrix and fiber-matrix interface debonding. However, for onset shear strength modelling, commonly only matrix failure is sufficient because matrix strengths are usually smaller than interface strengths for traditional FRP.

An example of functional failure due to matrix damage can be seen in Camanho et al.[48] Based on this consideration, the onset shear strength is selected

Figure 8. Continued.
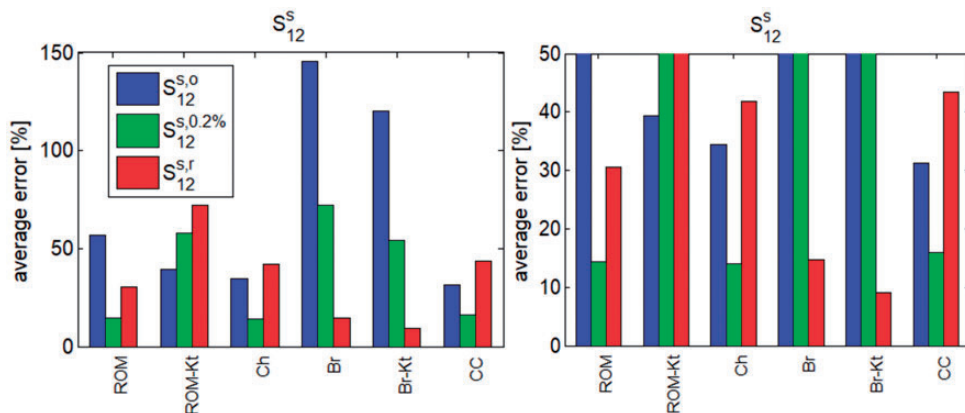
Figure 9. Average error for longitudinal shear strengths.

to evaluate the average error. Figure 10 presents the error ranges obtained by the different models presented showing that CC and Ch have very close results. Both have 20% of cases with errors smaller than 20%; 30% of cases with errors between 20% and 30%; 20% of cases with errors between 30% and 40%; and 30% of cases with errors between 40% and 50%. Note that considering the onset strength, Br and Br-Kt have 10% of cases with errors smaller than 10% and 90% of cases with errors higher than 50%. The unique case with error smaller than 10% is for the lamina T300/PR319, which demonstrates an unexpected linear behavior.

Logitudinal compressive strength

The model to estimate the longitudinal compressive strength is similar to the one presented for the tensile strength based on the ROM. Basically, the same hypothesis is adopted, replacing the fiber tensile strength by the fiber compressive strength. Under this assumption, the lamina longitudinal compressive strength is estimated by

$$S_{11}^c = \left[V_f + (1 - V_f) \left(\frac{E^m}{E_1^f} \right) \right] S_c^m \qquad (31)$$

This model is able to describe the fiber crushing. Nevertheless, some other failure mechanisms exist for compressive load parallel to fibers. Two main additional mechanisms are the fiber micro-buckling and kinking. Fiber micro-buckling is a consequence of elastic structural instability, such as the classical beam model in elastic foundation.[49] On the other hand, kinking is a consequence of matrix yielding due to initial

fiber misalignment or damage propagation. During kinking, the matrix around the misaligned fiber is subjected to shear. An analogy with the nonlinear response of the lamina subjected to longitudinal shear is discussed in Chaudhuri.[50] The main issue for the modeling of longitudinal compressive strength is to define the dominant failure mechanism.

The first effort for the modeling of fiber microbuckling was presented by Rosen.[51] Two buckling modes were evaluated: shear mode, where all fibers buckle in the same direction and the matrix is under shear; and extension mode when fibers buckle in opposite directions and matrix is under tension and compression. Usually, the shear mode takes place first and this mode can be considered from the engineering point of view.[52] For further discussion about extension mode see Andrianov et al.[47] The following equation defines the Rosen model:

$$S_{11}^c = \frac{G^m}{1 - V_f} \qquad (32)$$

Alternatively, Lo and Chim[53] modeled the fiber embedded in matrix as a Timoshenko beam. With respect to the boundary conditions, Lo and Chim employed a calibrated parameter and suggested that the estimation of the longitudinal compressive strength is given by

$$S_{11}^c = \frac{G_{12}}{1.5 + 12(6/\pi)^2 (G_{12}/E_1)} \qquad (33)$$

The longitudinal elastic modulus and the longitudinal shear modulus are estimated by the ROM and concentric cylinders models, respectively.[8]
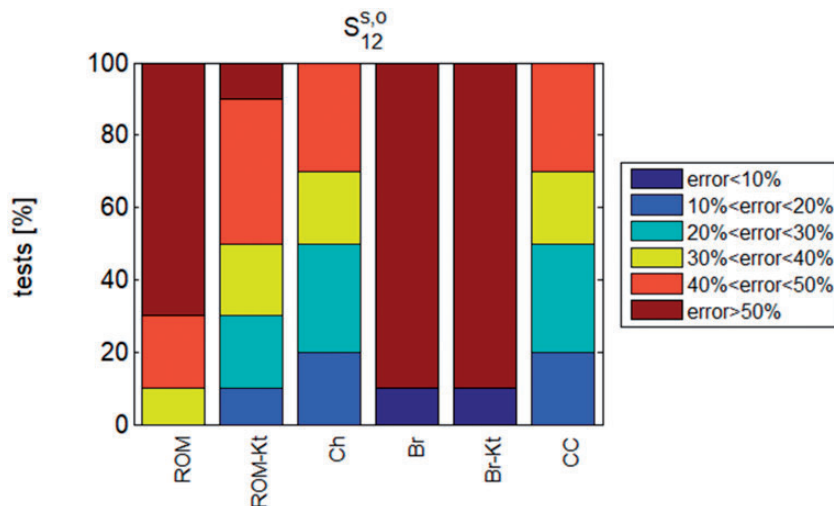

Figure 10. Error ranges for onset longitudinal shear strengths.

Argon[54] and Budiansky[55] considered matrix yield to model kinking. Argon employed a rigid perfectly plastic constitutive model while Budiansky employed an elastic perfectly plastic constitutive models. Budiansky and Fleck[56] proposed a generalized approach using Ramberg-Osgood equation to define matrix stress-strain relation and concluded that the elastic perfectly plastic model provided satisfactory estimations. Budiansky model is defined by the following equation:

$$S_{11}^c = \frac{G_{12}}{1 - (\phi/\gamma_Y)} \qquad (34)$$

where ϕ is the fiber initial misalignment and γ_Y is the strain at matrix yielding. According to Budiansky and Fleck,[56] $0 < \phi/\gamma_Y < 8$.

Barbero[57] defined the longitudinal shear stress-strain relation with a hyperbolic equation to model the region with fiber initial misalignment. Despite the complex equation derived, the following simplified equation is proposed by Barbero:

$$S_{11}^c = G_{12}\left(1 + 4.76\frac{G_{12}\phi}{S_{12}^s}\right)^{-0.69} \qquad (35)$$

Barbero[12] highlighted the importance of using the experimental values of G_{12} and S_{12}^s, and suggested that, in absence of experimental data, the concentric cylinders model can be used for G_{12} and the Chamis model for S_{12}^s. Based on the discussion presented in 'In-plane shear strength' section and keeping the model coherence, the expression derived for S_{12}^s using the concentric cylinders model is used in the present study instead of Chamis model. Hence, S_{12}^s is replaced by $S_{12}^{s,o}$ in the equation (35), where $S_{12}^{s,o}$ is computed by the equation (30). Despite this improvement of the Barbero model estimation for S_{11}^c using $S_{12}^{s,o}$ computed from concentric cylinder model instead of S_{12}^s computed from the Chamis model, both predictions are very close, as discussed in the previous section. Note that in this investigation the experimental value of S_{12}^s suggested by Barbero is named rupture shear strength.

Pimenta et al.[58] presented numerical and experimental investigations that are the basis of the analytical model developed by Pimenta et al.[59] According to the authors, the damage initiates around bent fiber misaligned where the matrix is under shear and the final failure is characterized by fiber rupture due to curvature. An alternative analysis of failure mechanism transition can be found in Gutkin et al.[60,61] Pimenta's model is defined by the following equation:

$$S_{11}^c = S_s^m\left[\frac{G_{2D}^m d_f + (\pi/L)^2 E_1^f I_f}{S_s^m + \pi(\bar{y}_0/L)G_{2D}^m}\right]\frac{V_f^{2D}}{A_f} \qquad (36)$$

where A_f and I_f are the fiber area and second moment of inertia per unit thickness and $\bar{y}_0$ and L are parameters defining the fiber misalignment. Additionally, the following 2D parameters are created to approximate the actual 3D condition:

$$G_{2D}^m = \frac{G^m}{1 - V_f^{2D}} \qquad (37)$$

$$V_f^{2D} = \frac{d_f}{d_f + t_m} \qquad (38)$$

$$t_m = d_f\left(\sqrt{\frac{\pi}{2\sqrt{3}V_f}} - 1\right) \qquad (39)$$

Alternatively, Aboudi and Gilat[62] and Gilat[63] studied fiber buckling using wave propagation techniques. Gutkin et al.[64,65] proposed a failure criterion for laminae subjected to longitudinal compression and shear combination. Numerically, Prabhakar and Waas[66] investigated the influence of the number of misaligned fibers on the lamina response. Barulich et al.[14] included 3D misalignment, concluding that the 2D representation has a good accuracy.

Adams[67], Joyce et al.[68] and Koerber and Camanho[69] discussed some difficulties of experimental procedures related to the geometry of specimen, tab influence and strain rate. The importance of the fiber misalignment is discussed in Wilhelmsson et al.,[70] and of the fiber curvature in Pimenta et al.[59] A novel model is developed assuming that fiber crushing failure is a combination of compression and bending.

Novel approach

A novel approach to evaluate the compressive strength is proposed based on the fiber crushing and misalignment. Failure is assumed to be due to a combination of axial and bending loads. Therefore, the novel model considers the curvature that introduces a bending moment in a misaligned fiber. Some authors assume a fiber sinusoidal misalignment.[14] Here, the fiber misaligned is assumed to have a following cubic form (see Figure 11):

$$x_2 = ax_1^3 + bx_1^2 + cx_1 + d \qquad (40)$$

The boundary conditions are assumed as follows: $u_2(0) = 0$, $\theta(0) = 0$, $\theta(L) = 0$ and $u_2(L) = u_{max}$, where $\theta = du_2/dx_1$. The maximum displacement, $u_2(L) = u_{max}$, is related to the maximum misalignment angle, $\theta_{max} = \phi$, where $\phi = 3u_{max}/2L$. Note that it is employed ϕ instead of u_{max} since it is the most usual
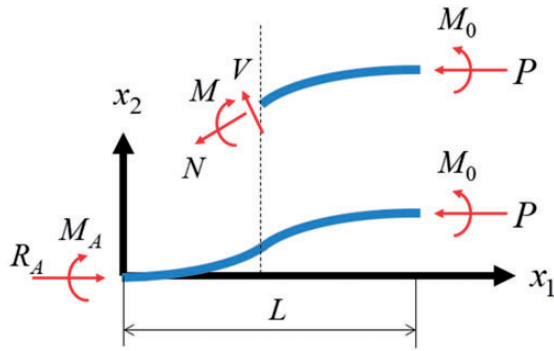
Figure 11. Representation of a single isolated fiber misaligned.

notation in the literature and a direct comparison with other models can be carried out. Using the maximum misalignment angle $\theta_{\max} = \phi$, equation (40) can be rewritten as follows:

$$u_2 = \frac{\phi}{L}\left(-\frac{4}{3L}x_1^3 + 2x_1^2\right) \quad (41)$$

Disregarding shear force effect and assuming that $\theta_{\max} < 5°$, the stored elastic strain energy on the fiber is

$$U = \int \left(\frac{M^2}{2E_1^f I_f} + \frac{N^2}{2E_1^f A_f}\right) dl$$

$$\cong \frac{\left(M_0^2 L + \frac{52}{315}P^2 L^3 \phi^2 - \frac{2}{3}M_0 P L^2 \phi\right)}{2E_1^f I_f}$$

$$+ \frac{P^2 L}{2E_1^f A_f} \quad (42)$$

By Castigliano's theorem, $\theta(L) = \partial U/\partial M_0 = 0$. Hence,

$$U = \frac{17}{315}\frac{P^2 L^3 \phi^2}{2E_1^f I_f} + \frac{P^2 L}{2E_1^f A_f} \quad (43)$$

In addition, Castigliano's theorem also establishes that the deflection on the point where the force is applied is

$$\delta = \frac{\partial U}{\partial P} = \left(\frac{17}{315}\frac{L^2 \phi^2}{I_f} + \frac{1}{A_f}\right)\frac{PL}{E_1^f} \quad (44)$$

Assuming that the maximum compressive stress on the fiber failure is $\sigma_f^{(\min)} = -S_c^f$, the critical compressive force is

$$P_c = -\left(1 + \frac{8}{3}\frac{L\phi}{d_f}\right)^{-1}\frac{\pi d_f^2}{4}S_c^f \quad (45)$$

Hence, the deflection during failure is

$$\delta_c = -\left[\frac{272}{315}\left(\frac{L\phi}{d_f}\right)^2 + 1\right]\left[1 + \frac{8}{3}\left(\frac{L\phi}{d_f}\right)\right]^{-1}\frac{L}{E_1^f}S_c^f \quad (46)$$

Equation (46) represents the fiber deflection to fail. However, it is still necessary to evaluate the applied macromechanical load to obtain this deflection. Prabhakar and Waas[71] presented a numerical model of the lamina with homogenized properties in the region where the fiber is perfectly aligned, and fibers and matrix are represented in the misaligned area. Considering that the misaligned region is small enough and therefore, it does not affect the macromechanical response of the lamina up to the failure, the macromechanical failure is defined by $\sigma_{11} = E_1 \varepsilon_{11} = E_1 \delta_c / L = -S_{11}^c$. Thus, replacing δ_c in equation (46),

$$S_{11}^c = \left[V_f + \left(\frac{E^m}{E_1^f}\right)(1 - V_f)\right]$$

$$\times \left[\frac{1 + (272/315)(L\phi/d_f)^2}{1 + (8/3)(L\phi/d_f)}\right]S_c^f \quad (47)$$

The longitudinal compressive strength assuming fiber crushing and including the influence of misalignment angle is defined by equation (47). A further study is required to define which value of $L\phi/d_f$ is representative of real structures.

Comparative analysis

Set of 61 experimental data from references listed in Table 2 is compiled (see Tables 7 and 8 in Appendix 1) and Figure 12 shows the average error variation according vs. $L\phi/d_f$. The minimum average error is 15%, that is obtained setting $L\phi/d_f = 0.09$ or $L\phi/d_f = 2.39$.

Replacing both $L\phi/d_f = 0.09$ and $L\phi/d_f = 2.39$ in the equation (47), $1 + (272/315)(L\phi/d_f)^2/1 + (8/3)(L\phi/d_f) \cong 0.8$. Note that it is equivalent to state that the fiber misalignment may reduce 20% of the longitudinal compressive strength considering fiber crushing failure mode. This proposed model is named *Rule of Mixture with misaligned fiber* (ROMmis), being defined by the following simplified equation:

$$S_{11}^c \cong 0.8\left[V_f + \left(\frac{E^m}{E_1^f}\right)(1 - V_f)\right]S_c^f \quad (48)$$

The similar calibration procedure presented for the proposed model is carried out for the Brabero,

Table 2. References used for the experimental data of the longitudinal compressive strength, S_{11}^c.

Reference	Fiber type
Barbero et al.[16]	Carbon
Falcó et al.[18]	Carbon
Hsiao and Daniel[19]	Carbon
Jumahat et al.[20]	Carbon
Kaddour and Hinton[21]	Carbon and glass
Kaddour et al.[22]	Carbon and glass
Perogamvros and Lampeas[24]	Carbon
Reddy et al.[25]	Glass
Soden et al.[26]	Carbon and glass
Wang et al.[27]	Carbon
Lo and Chim[53]	Carbon
Koerber and Camanho[69]	Carbon
Lee and Soutis[72]	Carbon
Thomson et al.[73]	Carbon

Table 3. Calibrated parameters of the models to estimate S_{11}^c.

Model	Calibrated parameters
Barbero (Bar)	$\phi = 0.5°$
Budiansky (Bud)	$\frac{\phi}{\gamma_Y} = 4.2$
Chamis (Ch)	$V_v = 0$
Pimenta (Pim)	$\frac{L}{y_0} = 121.8$
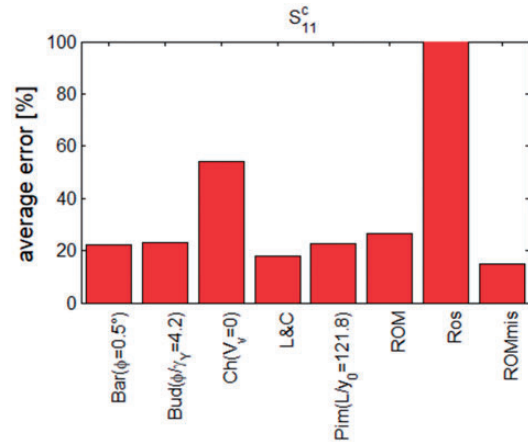
Figure 13. Average errors for longitudinal compressive strength.

Figure 12. Calibration of the proposed model for longitudinal compressive strength.

Budiansky, Chamis and Pimenta models. The calibrated parameters for each model are obtained minimizing the average errors compared with the compiled experimental data. The calibrated parameters are presented in the Table 3.

After the calibration of the models represented by parameters of the Table 3, a comparison among the models is performed. The average errors and the error ranges are evaluated comparing with the experimental data available in the literature (Table 2). All the discussed models are presented: Barbero (Bar), Budiansky (Bud), Lo and Chim (L&C), Chamis (Ch), Pimenta (Pim), rule of mixture (ROM), Rosin (Ros) and the novel modified rule of mixture including fiber misalignment (ROMmis). Figure 13 presents the average errors while Figure 14 shows the error ranges. Most of the models have average errors around 15% and 30%. Alternatively, these figures indicate the large

errors related to Ros model. Based on that, the following conclusions are highlighted:

(i) the newly proposed model, ROMmis, leads to the smallest average error (15%), resulting in an improvement of 11% with respect to the classical ROM with fiber misalignment effect;
(ii) Barbero, Budiansky and Lo and Chim models lead to an average error around 20%;
(iii) although it is not possible to state the dominant failure mechanism, the importance of the fiber misalignment must be highlighted and its influence on fiber crushing is verified by the novel model ROMmis;
(iv) among the top-rated models, Lo and Chim is the only one that does not consider fiber misalignment explicitly but has the advantage that it requires only elastic properties as input;
(v) Barbero, Lo and Chim and ROMmis models lead to over 40% of estimations with errors smaller than 10% and over 70% of estimations with errors smaller than 20%.

These results are in agreement with Naik and Kumar[74] that carried out a review study and recommended the use of the Lo and Chim and Budiansky models. The main difference is that more experimental and micromechanical models are used in the present study. Based on the current analysis, it is possible to
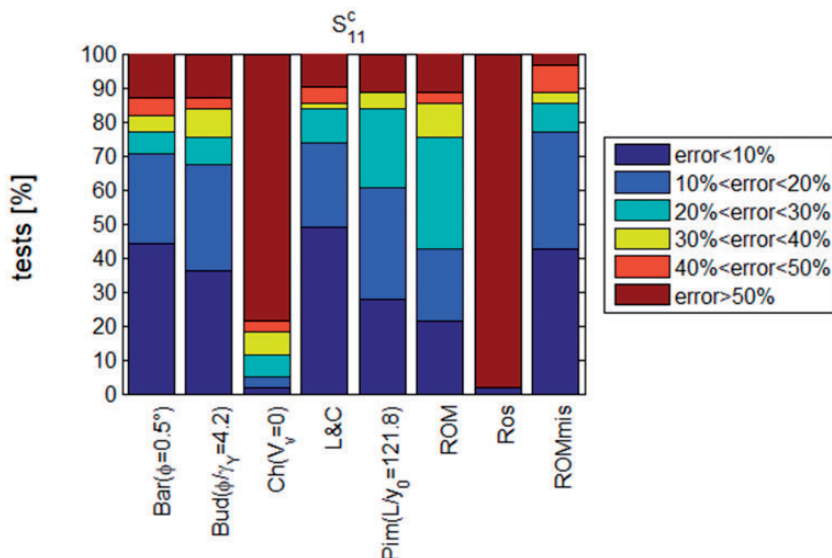
Figure 14. Error ranges for longitudinal compressive strength.

conclude that Lo and Chim and Budiansky, Barbero and ROMmis are the top-rated predictions, with an advantage of the novel ROMmis.

Note that there is model for the fiber-matrix interface. Based on the damage propagation sequence proposed by Pimenta et al.,[58] interface failure also can take place due to the excessive fiber curvature, increasing shear stress on the interface upto its limiting value, namely interface shear strength. For discussion on interface influence on the longitudinal compressive strength, see Zhou et al.[75]

Conclusions

An overview of micromechanical analytical models for longitudinal tension, compression and shear strengths of unidirectional laminae is presented. The improvements for the available modes are proposed by introducing the novel models for all three types of strength: ROM-based model considering the fiber strength reduction for tension; concentric cylinders model for onset shear; and the fiber misalignment effect for compression. A set of 98 experimental data is compiled and compared with analytical model estimations, where 27 are for longitudinal tensile strength S_{11}^t, 10 for in-plane shear strength S_{12}^s and 61 for longitudinal compressive strength S_{11}^c. ROM model's average error for S_{11}^t is 16.5% and it is decreased to 12.5% when the fiber strength reduction $r = 0.08$ is included. Regarding S_{12}^s, 6 models are evaluated, and it is shown that the concentric cylinders and Chamis models lead to the best predictions considering both onset and offset shear strength. Concentric cylinders model have an average error of 31.18% for onset strength, $S_{12}^{s,o}$, and 15.89% for offset strength, $S_{12}^{s,0.2\%}$.

Chamis model has an average error of 34.39% for onset strength, $S_{12}^{s,o}$, and 14.01% for offset strength, $S_{12}^{s,0.2\%}$. Finally, the proposed model for the longitudinal compressive strength S_{11}^c is compared with the other 7 approaches from the literature, and it is shown that it is the only one to provide the average error about 15%. Among the models known from the literature, Barbero, Budiansky and Lo and Chim models lead to the best predictions with the average errors around 20%.

Based on this analysis, it is possible to identify the importance of the micromechanics analysis on the strength prediction. And three newly proposed models present the best predictions in comparison with all alternatives available in the literature.

Declaration of Conflicting Interests

The author(s) declared no potential conflicts of interest with respect to the research, authorship, and/or publication of this article.

Funding

ORCID iDs

Pedro MCL Pacheco https://orcid.org/0000-0002-3374-5119
Alexander L Kalamkarov https://orcid.org/0000-0002-9964-5882

References

1. Soden PD, Kaddour AS and Hinton MJ. Recommendations for designers and researchers resulting from the world-wide failure exercise. *Compos Sci Technol* 2004; 64: 589–604.

2. Kaddour AS and Hinton MJ. Maturity of 3D failure criteria for fibre reinforced composites: comparison between theories and experiments: part B of WWFE-II. *J Compos Mater* 2013; 47: 925–966.

3. Kaddour AS, Hinton MJ, Smith PA, et al. The background to the third world-wide failure exercise. *J Compos Mater* 2013; 47: 2417–2426.

4. Chamis CC, Abdi F, Garg M, et al. Micromechanics-based progressive failure analysis prediction for WWFE-III composite coupon test cases. *J Compos Mater* 2013; 47: 2695–2712.

5. Huang ZM and Liu L. Predicting strength of fibrous laminates under triaxial loads only upon independently measured constituent properties. *Int J Mech Sci* 2014; 79: 105–129.

6. Tsai SW and Melo J. An invariant-based theory of composites. *Compos Sci Technol* 2014; 100: 237–243.

7. Andrianov IV, Awrejcewicz J and Danishevs'kyy VV. *Asymptotical mechanics of composites – modelling composites without FEM*. Berlin: Springer, 2018.

8. Vignoli LL, Savi MA, Pacheco P, et al. Comparative analysis of micromechanical models for the elastic composite laminae. *Compos Part B – Eng* 2019; 174: 106961.

9. Vignoli LL, Savi Ma Pacheco P and Kalamkarov AL. Micromechanical analysis of transversal strength of composite laminae. *Compos Struct*. Epub ahead of print 18 June 2020. DOI: 10.1016/j.compstruct.2020.112546

10. Tsai SW and Melo J. A unit circle failure criterion for carbon fiber reinforced polymer composites. *Compos Sci Technol* 2016; 123: 71–78.

11. Hart-Smith LJ. Expanding the capabilities of the ten-percent rule for predicting the strength of fibre–polymer composites. *Compos Sci Technol* 2002; 62: 1515–1544.

12. Barbero EJ. *Introduction to composite materials design*. 3rd ed. Boca Raton: CRC Press, 2018.

13. Zhang D and Waas AM. A micromechanics based multiscale model for nonlinear composites. *Acta Mech* 2014; 225: 1391–1417.

14. Barulich ND, Godoy LA and Barbero EJ. On microbuckling of unidirectional fiber-reinforced composites by means of computational micromechanics. *Lat Am J Solids Struct* 2016; 13: 3085–3106.

15. Aboudi J. Micromechanical analysis of the strength of unidirectional fiber composites. *Compos Sci Technol* 1988; 33: 79–96.

16. Barbero EJ, Abdelal GF and Caceres A. A micromechanics approach for damage modeling of polymer matrix composites. *Compos Struct* 2005; 67: 427–436.

17. Bogdanor MJ, Oskay C and Clay SB. Multiscale modeling of failure in composites under model parameter uncertainty. *Comput Mech* 2015; 56: 389–404.

18. Falcó O, Ávila RL, Tijs B, et al. Modelling and simulation methodology for unidirectional composite laminates in a Virtual Test Lab framework. *Compos Struct* 2018; 190: 137–159.

19. Hsiao HM and Daniel IM. Effect of fiber waviness on stiffness and strength reduction of unidirectional composites under compressive loading. *Compos Sci Technol* 1996; 56: 581–593.

20. Jumahat A, Soutis C and Hodzic A. A graphical method predicting the compressive strength of toughened unidirectional composite laminates. *Appl Compos Mater* 2011; 18: 65–83.

21. Kaddour AS and Hinton MJ. Input data for test cases used in benchmarking triaxial failure theories of composites. *J Compos Mater* 2012; 46: 2295–2312.

22. Kaddour AS, Hinton MJ, Smith PA, et al. Mechanical properties and details of composite laminates for the test cases used in the third world-wide failure exercise. *J Compos Mater* 2013; 47: 2427–2442.

23. Namdar O and Darendeliler H. Buckling, postbuckling and progressive failure analyses of composite laminated plates under compressive loading. *Composites Part B* 2017; 120: 143–151.

24. Perogamvros NG and Lampeas GN. Experimental and numerical investigation of AS4/8552 interlaminar shear strength under impact loading conditions. *J Compos Mater* 2016; 50: 2669–2685.

25. Reddy CV, Babu PR, Ramnarayanan R, et al. Mechanical characterization of unidirectional carbon and glass/epoxy reinforced composites for high strength applications. *Mater Today: Proc* 2017; 4: 3166–3172.

26. Soden PD, Hinton MJ and Kaddour AS. Lamina properties, lay-up configurations and loading conditions for a range of fibre-reinforced composite laminates. *Compos Sci Technol* 1998; 58: 1011–1022.

27. Wang J, Callus PJ and Bannister MK. and numerical investigation of the tension and compression strength of un-notched and notched quasi-isotropic laminates. *Structures* 2004; 64: 297–306.

28. Barbero EJ and Kelly KW. Predicting high temperature ultimate strength of continuous fiber metal matrix composites. *J Compos Mater* 1993; 27: 1214–1235.

29. Christensen R, Miyano Y and Nakada M. The size dependence of tensile strength for brittle isotropic materials and carbon fiber composite materials. *Compos Sci Technol* 2015; 106: 9–14.

30. Swolfs Y, Verpoest I and Gorbatikh L. Issues in strength models for unidirectional fibre-reinforced composites related to Weibull distributions, fibre packings and boundary effects. *Compos Sci Technol* 2015; 114: 42–49.

31. Swolfs Y, Verpoest I and Gorbatikh L. A review of input data and modelling assumptions in longitudinal strength models for unidirectional fibre-reinforced composites. *Compos Struct* 2016; 150: 153–172.

32. Timoshenko SP. *History of the strength of materials*. New York: McGraw-Hill, 1956.

33. Ha SK, Jin KK and Huang Y. Micro-mechanics of failure (MMF) for continuous fiber reinforced composites. *J Compos Mater* 2008; 42: 1873–1895.

34. ASTM D4762 – 18. Standard guide for testing polymer matrix composite materials.

35. Lubliner J. *Plasticity theory*. New York: Dover, 2008.

36. Castro JTP and Meggiolaro MA. *Fatigue design techniques: Vol. III – crack propagation, temperature and statistical Effects*. Scotts Valley, CA: CreateSpace Independent Publishing Platform, 2016.

37. Clay SB and Knoth PM. Experimental results of fatigue testing for calibration and validation of composite progressive damage analysis methods. *J Compos Mater* 2017; 51: 2083–2100.

38. Jumahat A, Soutis C, Jones FR, et al. Fracture mechanisms and failure analysis of carbon fibre/toughened epoxy composites subjected to compressive loading. *Compos Struct* 2010; 92: 295–305.

39. Laustsen S, Lund E, Kühlmeier L, et al. Interfibre failure characterisation of unidirectional and triax glass fibre non-crimp fabric reinforced epoxy laminates. *Appl Compos Mater* 2015; 22: 51–79.

40. Daniel IM and Ishai O. *Engineering mechanics of composite materials*. 2nd ed. Oxford: Oxford University Press, 2006.

41. Vignoli LL, Castro JTP and Meggiolaro MA. Stress concentration issues in unidirectional laminates. *J Braz Soc Mech Sci Eng* 2019b; 41: 462.

42. Devireddy SBR and Biswas S. Effect of fiber geometry and representative volume element on elastic and thermal properties of unidirectional fiber-reinforced composites. *J Compos* 2014; 2014: 1–12.

43. Huang ZM. Micromechanical prediction of ultimate strength of transversely isotropic fibrous composites. *Int J Solids Struct* 2001; 38: 4147–4172.

44. Huang ZM. On micromechanics approach to stiffness and strength of unidirectional composites. *J Reinf Plast Compos* 2019; 38: 167–196.

45. Christensen RM. *Mechanics of composite materials*. New York: Dover Publications, 2005.

46. Sokolnikoff IS. *Mathematical theory of elasticity*. 2nd ed. New York: McGraw-Hill Book Company, 1956.

47. Andrianov IV, Kalamkarov AL and Weichert D. Buckling of fibers in fiber-reinforced composites. *Composites: Part B* 2012; 43: 2058–2062.

48. Camanho PP, Dávila CG, Pinho ST, et al. of in situ strengths and matrix cracking in composites under transverse tension and in-plane shear. *Composites: Part A* 2006; 37: 165–176.

49. Timoshenko SP and Gere JM. *Theory of elastic stability*. 2nd ed. New York: Dover Publications, 2009.

50. Chaudhuri RA. A micro-kink theory for determination of shear modulus of a unidirectional composite lamina. *Compos Struct* 2010; 92: 395–400.

51. Rosen VW. *Mechanics of composite strengthening. Fibre composite materials*. Metals Park, OH: American Society of Materials, 1965.

52. Jones RM. *Mechanics of composite materials*. 2nd ed. Abingdon, UK: Taylor & Francis Editions, 1999.

53. Lo KH and Chim E. Compressive strength of unidirectional composites. *J Reinf Plast Compostes* 1992; 11: 838–896.

54. Argon AS. *Fracture of composites, treatise on materials science and technology*. New York: Academy Press, 1972.

55. Budiansky B. Micromechanics. *Comput Struct* 1983; 16: 3–12.

56. Budiansky B and Fleck NA. Compressive failure of fibre composite. *J Mech Phys Solids* 1993; 41: 183–211.

57. Barbero EJ. Prediction of compression strength of unidirectional polymer matrix composites. *J Compos Mater* 1998; 32: 483–502.

58. Pimenta S, Gutkin R, Pinho ST, et al. A micromechanical model for kink-band formation: part I – experimental study and numerical modelling. *Compos Sci Technol* 2009; 69: 948–955.

59. Pimenta S, Gutkin R, Pinho ST, et al. A micromechanical model for kink band formation: part II – analytical modelling. *Compos Sci Technol* 2009; 69: 956–964.

60. Gutkin R, Pinho ST, Robinson P, et al. On the transition from shear-driven fibre compressive failure to fibre kinking in notched CFRP laminates under longitudinal compression. *Compos Sci Technol* 2010; 70: 1223–1231.

61. Gutkin R, Pinho ST, Robinson P, et al. Micro-mechanical modelling of shear-driven fibre compressive failure and of fibre kinking for failure envelope generation in CFRP laminates. *Compos Sci Technol* 2010; 70: 1214–1222.

62. Aboudi J and Gilat R. Buckling analysis of fibers in composite materials by wave propagation analogy. *Int J Solids Struct* 2006; 43: 5168–5181.

63. Gilat R. A 3-D thermoelastic analysis of the buckling of a layer bonded to a compliant substrate and related problems. *Int J Solids Struct* 2010; 47: 2533–2542.

64. Gutkin R, Costa S and Olsson R. A physically based model for kink-band growth and longitudinal crushing of composites under 3D stress states accounting for friction. *Compos Sci Technol* 2016; 135: 39–45.

65. Gutkin R, Pinho ST, Robinson P, et al. A finite fracture mechanics formulation to predict fibre kinking and splitting in CFRP under combined longitudinal compression and in-plane shear. *Mech Mater* 2011; 43: 730–739.

66. Prabhakar P and Waas AM. Interaction between kinking and splitting in the compressive failure of unidirectional fiber reinforced laminated composites. *Compos Struct* 2013; 98: 85–92.

67. Adams DF. Tabbed versus untabbed fiber-reinforced composite compression specimens. In: Zureick A and Nettles AT (eds) *Composite materials: testing, design, and acceptance criteria*. West Conshohocken, PA: ASTM, 2002, pp. 3–16.

68. Joyce PJ, Violette MG and Moon MJ. Finite element analysis of unidirectional composite compression test specimens: a parametric study. In: Zureick A and Nettles AT (eds) *Composite materials: testing, design, and acceptance criteria*. West Conshohocken, PA: ASTM, 2002, pp. 30–68.

69. Koerber H and Camanho PP. High strain rate characterisation of unidirectional carbon–epoxy IM7-8552 in longitudinal compression. *Composites: Part A* 2011; 42: 462–470.

70. Wilhelmsson D, Talreja R, Gutkin R, et al. Compressive strength assessment of fibre composites based on a defect severity model. *Compos Sci Technol* 2019; 181: 107685.

71. Prabhakar P and Waas AM. Upscaling from a micromechanics model to capture laminate compressive strength due to kink banding instability. *Comput Mater Sci* 2013; 67: 40–47.

72. Lee J and Soutis C. A study on the compressive strength of thick carbon fibre-epoxy laminates. *Compos Sci Technol* 2007; 67: 2015–2026.

73. Thomson D, Cui H, Erice B, et al. A study on the longitudinal compression strength of fibre reinforced composites under uniaxial and off-axis loads using cross-ply laminate specimens. *Compos Part A* 2019; 121: 213–222.

74. Naik NK and Kumar RS. Compressive strength of unidirectional composites: evaluation and comparison of prediction models. *Compos Struct* 1999; 46: 299–308.

75. Zhou L, Zhao L, Liu F, et al. A micromechanical model for longitudinal compressive failure in unidirectional fiber reinforced composite. *Results Physics* 2018; 10: 841–848.

76. Ting Z, Lehua Q, Shaolin L, et al. Evaluation of the effect of PyC coating thickness on the mechanical properties of T700 carbon fiber tows. *Appl Surf Sci* 2019; 463: 310–321.

77. Kaddour AS, Hinton MJ and Soden PD. Behaviour of ± 45° glass/epoxy filament wound composite tubes under quasi-static equal biaxial tension – compression loading: experimental results. *Composites: Part B* 2003; 34: 689–704.

Appendix 1. Tabular data compiled from literature and model estimations.

This appendix aims to provide all the data compiled from the literature, considering fibers, matrices and laminae properties. Additionally, the obtained estimations from all discussed models are also presented. The references quoted in the Tables are related to the laminae properties, and the following additional references are used to obtain the matrix and fiber properties when they are not listed on the original references.[12,16,21,22,26,76]

Table 4. Compiled data and model estimations for S_{11}^t.

#	Reference	Matrix	Fiber	E^m (GPa)	E_1^f (GPa)	S_t^f (MPa)	V_f	$S_{11}^{t,exp}$ (MPa)	$S_{11}^t(r=0)$ (MPa)	$S_{11}^t(r=0.08)$ (MPa)
1	Kaddour and Hinton[21]	Epoxy	Carbon (AS)	3.2	231	3500	0.6	1990	2119.4	1949.8
2	Aboudi[15]	Epoxy (3501)	Carbon (AS4)	3.45	213.7	2250	0.66	1500	1497.4	1377.6
3	Falcó et al.[18]	Epoxy (8552)	Carbon (AS4)	4.08	231	3500	0.58	2106.4	2056	1891.5
4	Kaddour et al. (2013)[22]	Epoxy (3501-6)	Carbon (AS4)	4.2	231	3500	0.6	1950	2125.5	1955.4
5	Namdar and Darendeliler[23]	Epoxy (8552)	Carbon (AS4)	4.08	231	3500	0.55	1530	1952.8	1796.6
6	Perogamvros and Lampeas[24]	Epoxy (8552)	Carbon (AS4)	4.08	231	3500	0.57	2060	2021.6	1859.9
7	Soden et al.[26]	Epoxy (3501-6)	Carbon (AS4)	4.2	225	3350	.6	1950	2035	1872.2
8	Wang et al.[27]	Epoxy (3501-6)	Carbon (AS4)	4.2	231	3500	0.58	1950	2056.7	1892.2
9	Kaddour et al. (2013)	Epoxy (5260)	Carbon (G40-800)	3.45	290	5860	0.6	2750	3543.9	3260.4
10	Bogdanor et al.[17]	Epoxy (977-3)	Carbon (IM7)	3.55	276	5180	0.65	2785	3390.3	3119.1
11	Hsiao and Daniel[19]	Epoxy (3501-6)	Carbon (IM7)	5.1	276	5180	.66	2236	3451.3	3175.2
12	Jumahat et al.[20]	Epoxy (8551-7)	Carbon (IM7)	4.08	276	5180	0.54	2526	2832.4	2605.8
13	Kaddour and Hinton[21]	Epoxy (8551-7)	Carbon (IM7)	4.08	276	5180	0.6	2560	3138.6	2887.5
14	Kaddour et al. (2013)	Epoxy (8552)	Carbon (IM7)	4.08	276	5180	0.6	2560	3138.6	2887.5
15	Barbero et al.[16]	Epoxy (5208)	Carbon (T300)	4.6	230	2500	0.6	1550	1520	1398.4
16	Kaddour and Hinton[21]	Epoxy (PR319)	Carbon (T300)	0.95	231	2500	0.6	1378	1504.1	1383.8

(continued)

Table 4. Continued.

#	Reference	Matrix	Fiber	E^m (GPa)	E^f_1 (GPa)	S^f_t (MPa)	V_f	$S^{t,exp}_{11}$ (MPa)	$S^t_{11}(r=0)$ (MPa)	$S^t_{11}(r=0.08)$ (MPa)
17	Reddy et al.[25]	Epoxy (LY556)	Carbon (T300)	3.35	230	2500	0.59	1270.7	1489.9	1370.7
18	Soden et al.[26]	Epoxy (BSL914C)	Carbon (T300)	4	230	2500	.6	1500	1517.4	1396
19	Reddy et al.[25]	Epoxy (LY556)	Carbon (T700)	3.35	230	3900	0.58	1235.7	2285.9	2103
20	Kaddour et al. (2013)[22]	Epoxy (LY556)	Glass	3.35	74	2150	0.6	1280	1328.9	1222.6
21	Aboudi[15]	Epoxy	Glass (e-glass)	3.45	73	2150	0.6	1236	1330.6	1224.2
22	Kaddour and Hinton[21]	Epoxy (MY750)	Glass (e-glass)	3.35	74	2150	0.6	1280	1328.9	1222.6
23	Kaddour et al. (2003)[77]	Epoxy (MY750)	Glass (e-glass)	3.35	74	2150	0.6	1280	1328.9	1222.6
24	Reddy et al.[25]	Epoxy (LY556)	Glass (e-glass)	3.35	74	2150	0.7	930.3	1534.2	1411.5
25	Soden et al.[26]	Epoxy (LY556)	Glass (e-glass)	3.35	80	2150	.62	1140	1367.2	1257.8
26	Soden et al.[26]	Epoxy (MY750)	Glass (e-glass)	3.35	74	2150	.6	1280	1328.9	1222.6
27	Kaddour and Hinton[21]	Epoxy	Glass (S2-glass)	3.2	87	2850	0.6	1700	1751.9	1611.8

Table 5. Compiled data and model estimations for S^s_{12}.

#	Reference	Matrix	Fiber	G^m (GPa)	S^m_s (MPa)	G^f_{12} (GPa)	V_f	$S^{s,o}_{12}$ (MPa)	$S^{s,0.2}_{12}$ (MPa)	$S^{s,r}_{12}$ (MPa)
1	Soden et al.[26]	Epoxy (3501-6)	Carbon (AS4)	1.56	50	15	0.6	32.5	57.9	79
2	Soden et al.[26]	Epoxy (BSL914C)	Carbon (T300)	1.48	70	15	0.6	40	55.5	80
3	Soden et al.[26]	Epoxy (MY750)	Glass (e-glass)	1.24	54	30.8	0.6	34.98	48.1	72.99
4	Soden et al.[26]	Epoxy (LY556)	Glass (e-glass)	1.24	54	33.3	0.62	34.98	48.1	72.11
5	Kaddour and Hinton[21]	Epoxy (8551-7)	Carbon (IM7)	1.48	57	27	0.6	35	53.9	90
6	Kaddour and Hinton[21]	Epoxy	Glass (s-glass)	1.2	52	36	0.6	29.34	46	72.99
7	Kaddour and Hinton[21]	Epoxy	Carbon (AS)	1.2	50	15	0.6	30	45.2	70
8	Kaddour and Hinton[21]	Epoxy (PR319)	Carbon (T300)	0.35	41	15	0.6	65	65	65
9	Kaddour et al. (2013)	Epoxy (8552)	Carbon (IM7)	1.48	57	27	0.6	40	53.9	90
10	Kaddour et al. (2013)	Epoxy (5260)	Carbon (G40800)	1.28	57	27	0.6	40	52.8	90

Table 6. Compiled data and model estimations for S_{12}^s.

	S_{12}^s (MPa)					
#	ROM	ROM-Kt	Ch	Br	Br-Kt	CC
1	50	23.5	42.2	79.1	70.5	41
2	70	32.4	59	111.3	99.2	57.4
3	54	20.5	45	90.2	80.7	43.6
4	54	19.4	45.3	91.7	81	44.1
5	57	22.9	47.6	94	84	46.2
6	52	19.2	43.2	87.4	78.3	41.9
7	50	21.9	42	80.7	72	40.8
8	41	14.5	34	69.6	62.3	33
9	57	22.9	47.6	94	84	46.2
10	57	22.3	47.5	94.6	84.6	46.1

Table 7. Compiled data and model estimations for S_{11}^c.

#	Reference	Matrix	Fiber	E^m (GPa)	ν^m	S_s^m (MPa)	E_1^f (GPa)	G_{12}^f (GPa)	ν_{12}^f	S_c^f (MPa)	d_f (mm)	V_f	$S_{11}^{c,exp}$ (MPa)
1	Lo and Chim[53]	Epoxy (3501-6)	Carbon (AS)	4.3	0.34	50	214	13.8	0.2	3000	7	0.52	1280
2	Lo and Chim[53]	Epoxy (3501-6)	Carbon (AS)	4.3	0.34	50	214	13.8	0.2	3000	7	0.55	1329
3	Lo and Chim[53]	Epoxy (3501-6)	Carbon (AS)	4.3	0.34	50	214	13.8	0.2	3000	7	0.57	1420
4	Lo and Chim[53]	Epoxy (3501-6)	Carbon (AS)	4.3	0.34	50	214	13.8	0.2	3000	7	0.58	1390
5	Lo and Chim[53]	Epoxy (3501-6)	Carbon (AS)	4.3	0.34	50	214	13.8	0.2	3000	7	0.62	1791
6	Lo and Chim[53]	Epoxy (3501-6)	Carbon (AS)	4.3	0.34	50	214	13.8	0.2	3000	7	0.66	1447
7	Kaddour and Hinton[21]	Epoxy	Carbon (AS)	3.2	0.35	50	231	15	0.2	3000	7	0.6	1500
8	Soden et al.[26]	Epoxy (3501-6)	Carbon (AS4)	4.2	.35	50	225	15	0.2	2500	7	0.6	1480
9	Wang et al.[27]	Epoxy (3501-6)	Carbon (AS4)	4.2	.35	50	231	15	0.2	3000	7	0.62	1507
10	Kaddour et al. (2013)	Epoxy (3501-6)	Carbon (AS4)	4.2	0.34	50	231	15	0.2	3000	7	0.6	1480
11	Perogamvros and Lampeas[24]	Epoxy (8552)	Carbon (AS4)	4.08	0.38	57	231	15	0.2	3000	7	0.58	1570
12	Falcó et al.[18]	Epoxy (8552)	Carbon (AS4)	4.08	0.38	57	231	15	0.2	3000	7	0.59	1675.9
13	Kaddour et al. (2013)	Epoxy (5260)	Carbon (G40-800)	3.45	0.35	57	290	27	0.2	3200	8	0.6	1700
14	Hsiao and Daniel[19]	Epoxy (3501-6)	Carbon (IM7)	4.3	0.35	50	276	27	0.2	3200	4.5	.66	1682
15	Lee and Soutis[72]	Epoxy (8552)	Carbon (IM7)	4.08	0.38	57	276	27	0.2	3200	4.5	0.66	1690
16	Lee and Soutis[72]	Epoxy (8552)	Carbon (IM7)	4.08	0.38	57	276	27	0.2	3200	4.5	0.56	1570
17	Lee and Soutis[72]	Epoxy (8552)	Carbon (IM7)	4.08	0.38	57	276	27	0.2	3200	4.5	0.54	1253
18	Lee and Soutis[72]	epoxy (8552)	carbon (IM7)	4.08	0.38	57	276	27	0.2	3200	4.5	0.57	869
19	Koerber and Camanho[69]	Epoxy (8552)	Carbon (IM7)	4.08	0.38	57	276	27	0.2	3200	4.5	0.57	1018
20	Koerber and Camanho[69]	Epoxy (8552)	Carbon (IM7)	4.08	0.38	57	276	27	0.2	3200	4.5	0.55	1002
21	Koerber and Camanho[69]	Epoxy (8552)	Carbon (IM7)	4.08	0.38	57	276	27	0.2	3200	4.5	0.53	946
22	Koerber and Camanho[69]	Epoxy (8552)	Carbon (IM7)	4.08	0.38	57	276	27	0.2	3200	4.5	0.56	1093
23	Jumahat et al.[20]	Epoxy (8551-7)	Carbon (IM7)	4.08	0.38	57	276	27	0.2	3200	4.5	0.54	916
24	Kaddour and Hinton[21]	Epoxy (8551-7)	Carbon (IM7)	4.08	0.38	57	276	27	0.2	3200	4.5	0.6	1590
25	Kaddour et al. (2013)	Epoxy (8552)	Carbon (IM7)	4.08	0.38	57	276	27	0.2	3200	4.5	0.6	1590
26	Thomson et al.[73]	Epoxy (8552)	Carbon (IM7)	4.08	0.38	57	276	27	0.2	3200	4.5	0.58	1499
27	Thomson et al.[73]	Epoxy (8552)	Carbon (IM7)	4.08	0.38	57	276	27	0.2	3200	4.5	0.58	1340
28	Thomson et al.[73]	Epoxy (8552)	Carbon (IM7)	4.08	0.38	57	276	27	0.2	3200	4.5	0.58	1659
29	Thomson et al.[73]	Epoxy (8552)	Carbon (IM7)	4.08	0.38	57	276	27	0.2	3200	4.5	0.58	1873
30	Thomson et al.[73]	Epoxy (8552)	Carbon (IM7)	4.08	0.38	57	276	27	0.2	3200	4.5	0.58	1790
31	Thomson et al.[73]	Epoxy (8552)	Carbon (IM7)	4.08	0.38	57	276	27	0.2	3200	4.5	0.58	1710
32	Thomson et al.[73]	Epoxy (8552)	Carbon (IM7)	4.08	0.38	57	276	27	0.2	3200	4.5	0.58	1683
33	Thomson et al.[73]	Epoxy (8552)	Carbon (IM7)	4.08	0.38	57	276	27	0.2	3200	4.5	0.58	1773

(continued)

Table 7. Continued.

#	Reference	Matrix	Fiber	E^m (GPa)	ν^m	S_s^m (MPa)	E_1^f (GPa)	G_{12}^f (GPa)	ν_{12}^f	S_c^f (MPa)	d_f (mm)	V_f	$S_{11}^{c,exp}$ (MPa)
34	Thomson et al.[73]	Epoxy (8552)	Carbon (IM7)	4.08	0.38	57	276	27	0.2	3200	4.5	0.58	1506
35	Thomson et al.[73]	Epoxy (8552)	Carbon (IM7)	4.08	0.38	57	276	27	0.2	3200	4.5	0.58	1772
36	Thomson et al.[73]	Epoxy (8552)	Carbon (IM7)	4.08	0.38	57	276	27	0.2	3200	4.5	0.58	1462
37	Thomson et al.[73]	Epoxy (8552)	carbon (IM7)	4.08	0.38	57	276	27	0.2	3200	4.5	0.58	1283
38	Thomson et al.[73]	Epoxy (8552)	Carbon (IM7)	4.08	0.38	57	276	27	0.2	3200	4.5	0.58	1651
39	Thomson et al.[73]	Epoxy (8552)	Carbon (IM7)	4.08	0.38	57	276	27	0.2	3200	4.5	0.58	1558
40	Thomson et al.[73]	Epoxy (8552)	Carbon (IM7)	4.08	0.38	57	276	27	0.2	3200	4.5	0.58	1710
41	Thomson et al.[73]	epoxy (8552)	carbon (IM7)	4.08	0.38	57	276	27	0.2	3200	4.5	0.58	1661
42	Thomson et al.[73]	Epoxy (8552)	Carbon (IM7)	4.08	0.38	57	276	27	0.2	3200	4.5	0.58	1423
43	Thomson et al.[73]	Epoxy (8552)	carbon (IM7)	4.08	0.38	57	276	27	0.2	3200	4.5	0.58	1463
44	Thomson et al.[73]	Epoxy (8552)	Carbon (IM7)	4.08	0.38	57	276	27	0.2	3200	4.5	0.58	1469
45	Lo and Chim[53]	Epoxy (5208)	Carbon (T300)	4	0.35	51.6	221	8.96	0.2	2000	7	0.55	1570
46	Lo and Chim[53]	Epoxy (5208)	Carbon (T300)	4	0.35	51.6	221	8.96	0.2	2000	7	0.59	1177
47	Lo and Chim[53]	Epoxy (5208)	Carbon (T300)	4	0.35	51.6	221	8.96	0.2	2000	7	0.59	1280
48	Lo and Chim[53]	Epoxy (5208)	Carbon (T300)	4	0.35	51.6	221	8.96	0.2	2000	7	0.62	1309
49	Lo and Chim[53]	Epoxy (5208)	Carbon (T300)	4	0.35	51.6	221	8.96	0.2	2000	7	0.62	1723
50	Lo and Chim[53]	Epoxy (5208)	Carbon (T300)	4	0.35	51.6	221	8.96	0.2	2000	7	0.65	1585
51	Lo and Chim[53]	Epoxy (5208)	Carbon (T300)	4	0.35	51.6	221	8.96	0.2	2000	7	0.66	1508
52	Lo and Chim[53]	Epoxy (5208)	Carbon (T300)	4	0.35	51.6	221	8.96	0.2	2000	7	0.7	1500
53	Soden et al.[26]	Epoxy (BSL914C)	Carbon (T300)	4	.35	70	230	15	.2	2000	7	0.6	900
54	Barbero et al.[16]	Epoxy (5208)	Carbon (T300)	4.6	0.38	51.6	230	15	.2	2000	7	0.6	1096
55	Kaddour and Hinton[21]	Epoxy (PR319)	Carbon (T300)	0.95	0.35	41	231	15	0.2	2000	7	0.6	950
56	Kaddour et al. (2013)	Epoxy (LY556)	Glass	3.35	0.35	54	74	30.8	0.2	1450	11	0.6	800
57	Soden et al.[26]	Epoxy (MY750)	Glass (e-glass)	3.35	.35	54	74	30.8	.2	1450	11	0.6	800
58	Kaddour and Hinton[21]	Epoxy (MY750)	Glass (e-glass)	3.35	0.35	54	74	30.8	0.2	1450	11	0.6	800
59	Reddy et al.[25]	epoxy (LY556)	glass (e-glass)	3.35	0.35	54	74	30.8	.2	1450	11	0.7	721.8
60	Soden et al.[26]	Epoxy (LY556)	Glass (e-glass)	3.35	.35	54	80	33.33	.2	1450	11	0.62	570
61	Kaddour and Hinton[21]	Epoxy	Glass (S2-glass)	3.2	0.35	52	87	36	0.2	2450	11	0.6	1150

Table 8. Compiled data and models estimations for S_{11}^c.

	S_{11}^c (MPa)							
#	Bar ($\phi = 0.5°$)	Bud ($\phi/\gamma = 4.2$)	Ch ($V_v = 0$)	L&C	Pim ($L/y_0 = 121.8$)	ROM	Ros	ROM-mis
1	1257.8	1203.1	536.14	1289	1135.7	1588.9	3342.7	1271.1
2	1302.6	1274.8	540.33	1363.2	1192	1677.1	3565.5	1341.7
3	1333.6	1326.1	543.26	1414.5	1229.9	1735.9	3731.3	1388.7
4	1349.4	1352.8	544.77	1440.7	1249	1765.3	3820.2	1412.3
5	1415.3	1468.1	551.03	1550	1326.3	1882.9	4222.3	1506.3
6	1485.7	1598.8	557.66	1666.9	1405.3	2000.5	4719.1	1600.4
7	1255.2	1147.9	544.6	1386.5	1208.8	1816.6	2963	1453.3
8	1380	1410	546.75	1532.1	1280.1	1518.7	3888.9	1214.9
9	1414.6	1472	549.98	1611.1	1319.1	1880.7	4093.6	1504.6
10	1383.4	1417.7	546.82	1556	1281.9	1821.8	3917.9	1457.5
11	1422.3	1301	619.2	1464.4	1360.9	1762.3	3519.7	1409.8
12	1440.5	1329.1	620.98	1492.6	1383.5	1791.7	3605.5	1433.4
13	1449.4	1358.9	617.69	1682	1359.9	1935.2	3194.4	1548.2
14	1588.9	1909.4	553.29	2066.6	1403.6	2129	4684.1	1703.2
15	1672.6	1799.7	630.39	2004.3	1546.6	2128.1	4347.8	1702.5
16	1448	1392.8	611.03	1622.1	1316.1	1812.8	3359.7	1450.3

(continued)

Table 8. Continued.

	$S_{11}^{c_i}$ (MPa)							
#	Bar ($\phi = 0.5°$)	Bud ($\phi/\gamma = 4.2$)	Ch ($V_v = 0$)	L&C	Pim ($L/y_0 = 121.8$)	ROM	Ros	ROM-mis
17	1408.3	1328.4	607.52	1555.4	1272	1749.8	3213.6	1399.8
18	1468.4	1426.8	612.83	1656.4	1338.4	1844.3	3437.8	1475.5
19	1468.4	1426.8	612.83	1656.4	1338.4	1844.3	3437.8	1475.5
20	1427.9	1360	609.26	1588.4	1293.9	1781.3	3285	1425
21	1389	1297.8	605.81	1523.1	1250.1	1718.2	3145.2	1374.6
22	1448	1392.8	611.03	1622.1	1316.1	1812.8	3359.7	1450.3
23	1408.3	1328.4	607.52	1555.4	1272	1749.8	3213.6	1399.8
24	1532.2	1536.6	618.43	1764.3	1406.2	1938.9	3695.7	1551.1
25	1532.2	1536.6	618.43	1764.3	1406.2	1938.9	3695.7	1551.1
26	1489.3	1462	614.67	1691.6	1360.8	1875.9	3519.7	1500.7
27	1489.3	1462	614.67	1691.6	1360.8	1875.9	3519.7	1500.7
28	1489.3	1462	614.67	1691.6	1360.8	1875.9	3519.7	1500.7
29	1489.3	1462	614.67	1691.6	1360.8	1875.9	3519.7	1500.7
30	1489.3	1462	614.67	1691.6	1360.8	1875.9	3519.7	1500.7
31	1489.3	1462	614.67	1691.6	1360.8	1875.9	3519.7	1500.7
32	1489.3	1462	614.67	1691.6	1360.8	1875.9	3519.7	1500.7
33	1489.3	1462	614.67	1691.6	1360.8	1875.9	3519.7	1500.7
34	1489.3	1462	614.67	1691.6	1360.8	1875.9	3519.7	1500.7
35	1489.3	1462	614.67	1691.6	1360.8	1875.9	3519.7	1500.7
36	1489.3	1462	614.67	1691.6	1360.8	1875.9	3519.7	1500.7
37	1489.3	1462	614.67	1691.6	1360.8	1875.9	3519.7	1500.7
38	1489.3	1462	614.67	1691.6	1360.8	1875.9	3519.7	1500.7
39	1489.3	1462	614.67	1691.6	1360.8	1875.9	3519.7	1500.7
40	1489.3	1462	614.67	1691.6	1360.8	1875.9	3519.7	1500.7
41	1489.3	1462	614.67	1691.6	1360.8	1875.9	3519.7	1500.7
42	1489.3	1462	614.67	1691.6	1360.8	1875.9	3519.7	1500.7
43	1489.3	1462	614.67	1691.6	1360.8	1875.9	3519.7	1500.7
44	1489.3	1462	614.67	1691.6	1360.8	1875.9	3519.7	1500.7
45	1230.2	1064.8	562.47	1257.7	1200.3	1116.3	3292.2	893
46	1284.1	1140.6	568.29	1346.8	1280.2	1194.8	3613.4	955.9
47	1284.1	1140.6	568.29	1346.8	1280.2	1194.8	3613.4	955.9
48	1326.4	1202.6	572.9	1417	1341.4	1253.8	3898.6	1003
49	1326.4	1202.6	572.9	1417	1341.4	1253.8	3898.6	1003
50	1370.5	1269.5	577.72	1490.3	1403.9	1312.7	4232.8	1050.1
51	1385.6	1293.1	579.36	1515.5	1425	1332.3	4357.3	1065.8
52	1448.4	1393.9	586.14	1620.6	1510.9	1410.9	4938.3	1128.7
53	1630.2	1360.2	764.85	1519.4	1646.1	1213.9	3703.7	971.1
54	1437.1	1482.4	564.92	1589.3	1330.2	1216	4166.7	972.8
55	664.2	404.4	442.59	678.5	702.1	1203.3	879.6	962.6
56	1400.9	1349.1	584.52	766.6	1295.9	896.3	3101.9	717
57	1400.9	1349.1	584.52	766.6	1295.9	896.3	3101.9	717
58	1400.9	1349.1	584.52	766.6	1295.9	896.3	3101.9	717
59	1640.6	1801.5	604.18	918.2	1527.4	1034.7	4135.8	827.8
60	1450.4	1439	587.97	843.1	1340.4	922.1	3265.1	737.7
61	1357.1	1319.9	562.2	852.1	1245.5	1506	2963	1204.8